PHARMACEUTICS, PREFORMULATION AND DRUG DELIVERY

Physicochemical, Crystallographic, Thermal, and Spectroscopic Behavior of Crystalline and X-ray Amorphous Ciclesonide

MARTIN PHILIPP FETH, JÜRGEN VOLZ, URSULA HESS, ERNST STURM, ROLF-PETER HUMMEL

NYCOMED GmbH, Byk-Gulden-Str. 2, D-78467 Konstanz, Germany

Received 20 August 2007; revised 5 September 2007; accepted 7 September 2007

Published online in Wiley InterScience (www.interscience.wiley.com). DOI 10.1002/jps.21223

ABSTRACT: Single crystal structure experiments revealed that the orthorhombic needles of Ciclesonide crystallized in $P2_12_12_1$ space group with four independent molecules in the unit cell. Amorphous Ciclesonide was prepared by lyophilization and characterized in comparison with crystalline material by differential scanning calorimetry (DSC), Fourier transformed (FT)-Raman spectroscopy, powder X-ray diffraction, dissolution, and saturation solubility experiments. Significant differences in the dissolution, thermal, and spectrometric behavior were observed for both solid-state phases. DSC- and FT-Raman methods for the determination of amorphous content in crystalline Ciclesonide samples were established. Isothermal and dynamical recrystallization studies on amorphous Ciclesonide were conducted using dispersive hot-stage Raman microscopy. The recrystallization was observed to be a two-step process with an induction period (most likely nuclei formation) followed by the actual recrystallization (crystal growth). The recrystallization rate constants and Avrami exponents ($n = 2$) were determined from the isothermal experiments at various temperatures using Johnson–Mehl–Avrami theory. Isothermal activation energies were obtained from Arrhenius plots using the temperature dependence of (a) the rate constants (160.4 kJ/mol) and (b) the induction time (140.9 kJ/mol) of the isothermal hot-stage experiments. J Pharm Sci 97:3765–3780, 2008

Keywords: Ciclesonide; crystal structure; amorphous; recrystallization; Avrami kinetics; dissolution behavior; differential scanning calorimetry (DSC); FT-Raman spectroscopy; dispersive Raman hot-stage microscopy

INTRODUCTION

A major issue in pharmaceutical sciences today is to increase the dissolution rate and bioavailability of poorly soluble drugs. A possible approach is the use of dosage forms containing amorphous material of the active ingredient,[1–4] which possesses a higher dissolution rate and apparent solubility than its crystalline counterpart.[5] The amorphous state, however, is thermodynamically metastable,

This article contains supplementary material, available at www.interscience.wiley.com/jpages/0022-3549/suppmat.

Correspondence to: Martin Philipp Feth (Telephone: +49-7531-84-4343; Fax: +49-7531-84-94343; E-mail: martin.feth@gmx.de)

Journal of Pharmaceutical Sciences, Vol. 97, 3765–3780 (2008)

thus amorphous systems tend to spontaneous transformations into the crystalline state.[6–8] This can be very critical for the pharmaceutical product, as the bioavailability and therefore also the product efficacy may be affected in case that the recrystallization process occurs during the shelf-life of the product. It also has to be taken into consideration that the use of amorphous material might have a crucial impact on other physico-chemical parameters of the compound such as the hygroscopicity, mechanical, and flow parameters as well as chemical stability in the solid state.[9] For these reasons it is necessary to establish suitable analytical and spectroscopic methods for the detection, characterization, and quantification of amorphous materials. Up to now many techniques have been described in the literature for the detection and quantification of amorphous content as well as for the characterization of the isothermal and non-isothermal recrystallization behavior of compounds in the amorphous state. Powder X-ray diffraction,[10] near IR-[11] or Fourier transformed (FT)-Raman spectroscopy,[9] microcalorimetry,[12,13] solution calorimetry,[14] differential scanning calorimetry (DSC),[15–17] and gravimetry[18] were successfully applied to study such systems.

In this study, we investigated crystalline and amorphous Ciclesonide (refer to Fig. 1) by means of single crystal and powder X-ray diffraction, DSC, FT-Raman spectroscopy, and dispersive hot-stage Raman microscopy. The dissolution behavior in water at 37°C of both crystalline and X-ray amorphous Ciclesonide was studied in order to demonstrate the impact of amorphicity on physicochemical properties.

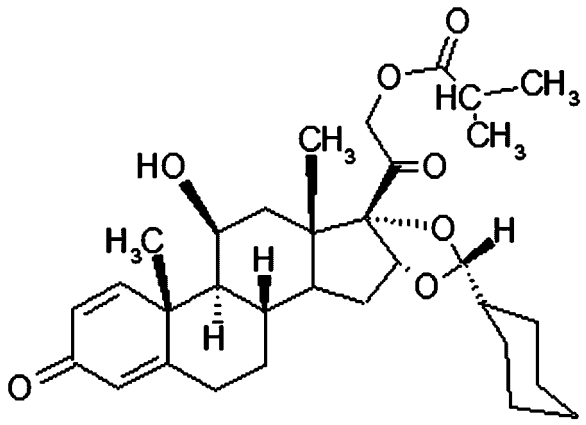

Figure 1. Chemical structure of 16,17-[(cyclohexylmethylene)bis(oxy)]-11-hydroxy-21-(2-methyl-1-oxopropoxy)-pregna-1,4-diene-3,20-dione[11β,16α(R)] (Ciclesonide).

FT-Raman and DSC methods for the quantification of amorphous content in "crystalline" Ciclesonide batches were established and tested in a comparative manner.

Finally the isothermal recrystallization kinetics of amorphous Ciclesonide was studied in detail using dispersive hot-stage Raman microscopy, a method rarely used for the investigation of such phenomena. Johnson–Avrami–Mehl theory has been applied to determine the crystallization rate constants. Activation energies were obtained from Arrhenius analysis of the data.

EXPERIMENTAL PART

Single Crystal X-ray Diffraction

A crystal ($0.8 \times 0.015 \times 0.01$ mm^3) was measured at $T = 298(2)$ K on a Stoe IPDS diffractometer using the Mo-Kα radiation ($\lambda = 0.71073$ Å). The measured theta range was 1.90°–24.39°. All crystallographic calculations were carried out using the SHELXLT program package, refinement was carried out using the full-matrix least squares method.[19] The positions of the hydrogen atoms were refined isotropically. This gave a goodness-of-fit of 0.764 and the following R-values ($I > 2\sigma(I)$): R1 = 0.0494, wR2: 0.0896.

Crystallographic data for the structure analysis have been deposited with the Cambridge Crystallographic Data Centre, CCDC No. 656903. Copies of this information may be obtained free of charge from: The Director, CCDC, 12 Union Road, Cambridge, CB21EZ UK (fax: +44-1223-336-033; e-mail: deposit@ccdc.cam.ac.uk www://www.ccdc.cam.ac.uk).

FT-Raman Spectroscopy

FT-Raman spectra were recorded on a Bruker Optics RAM II module, which was coupled to a Bruker Optics Vertex 70 FT-IR spectrometer. The RAM II module was equipped with a liquid nitrogen cooled high sensitivity germanium detector (D-418 TF) and a diode pumped 500 mW Nd:YAG laser (wavelength: 1064 nm). Data acquisition and analysis were performed using the software package OPUS 5.4 from Bruker Optics. For each spectrum 512 scans were collected in 180° reflection mode using a spectral resolution of 2 cm^{-1} in order to provide Raman spectra with a low S/N ratio in combination with well-resolved Raman signals. To avoid heating of the colorless samples the laser power was set to a

value of 100 mW. The sample preparation consisted of gently compacting the powders into a cylindrical aluminum sample pan (height: 4 mm, diameter: 10 mm) with a pinhole (diameter: 2 mm, depth: 1 mm). The calculations of the different Raman intensity ratios, e.g., $I_{1604\,cm^{-1}}/I_{804\,cm^{-1}}$, were performed directly from the FT-Raman spectra without carrying out an background correction.

Dispersive (Hot-Stage) Raman Microscopy

Dispersive Raman microscopy has been performed on a Bruker Senterra confocal system based on an Olympus BX51 optical microscope equipped with a 785 nm laser diode (laser power: 100 mW) as source, an Andor iDUS DV420A CCD camera (peltier-cooled, working temperature: -50°C) as detector and a motorized XYZ stage for mapping and confocal experiments. The frequency calibration of the system was performed automatically using neon emission lines (Sure_Cal technology). The microscopic Raman measurements were performed with a 20-fold magnification long-distance objective from Olympus. Data acquisition and analysis were performed using the software package OPUS 5.5 from Bruker Optics. For each spectrum two spectral regions 2600–1480 and 1500–90 cm^{-1} were measured (Raman acquisition time per spectral region: 20 s, repeats per spectral region: 3, total acquisition time: 314 s) with a spectral resolution of 3–5 cm^{-1}. Afterwards the overlapping spectral regions were mathematically merged by an automated program routine. For the hot-stage Raman experiments a Linkam Thermostage THMS 600 was used. The temperature at the sample was checked using a Fluke Thermocouple Thermometer 51 II equipped with a Fluke beaded K-type thermocouple. The accuracy of the attuned temperature was found to be within $\pm 0.5^{\circ}$C. Temperature stability during the isothermal experiments was $\pm 0.1^{\circ}$C. For the measurements about 1.0–1.5 mg of the amorphous powders were gently compacted into an aluminum sample pan (height: 2 mm, diameter: 10 mm, weight: 395.8 mg) with a pinhole (diameter: 2 mm, depth: 1 mm) and placed in the sample holder of the thermostage and measured through the quartz glass window of the thermostage. Two different types of experiments were carried out: (1) temperature ramps between 50 and 140°C in 1°C temperature steps (equilibration time before the Raman measurement: 20 s, measurement time at a certain temperature: 334 s) and (2) isothermal Raman experiments at 65, 90, 100, 104, 106, 108, 110, 112, 114, and 115°C (heating rate to the starting temperature 10 K/min) in dependence of time (time delay between the end of each measurement: 324 s = 5.4 min). The calculation of the Raman intensity ratio $I_{1603\,cm^{-1}}/I_{802\,cm^{-1}}$ was performed directly from the Raman spectra without carrying out an background correction, assuming a spectral-independent background. The relative crystallinity X, which is necessary for the Avrami plots and the Avrami coefficient determination, was calculated from the intensity ratio $I_{1603\,cm^{-1}}/I_{802\,cm^{-1}}$, as with this ratio a linear behavior between the relative crystallinity X and the intensity ratio (X-range: 0–100%) was observed by FT-Raman investigations on spiked Ciclesonide samples.

PXRD, DSC, TG, and ^{1}H-NMR Spectroscopy

The XRD experiments in reflection mode were performed on a STOE STADI P diffractometer equipped with a Ge(111) monochromator and a linear PSD detector over an angular range of $2\theta = 3^{\circ}$–40° (angular step size: 0.2°, measurement time per step: 15 s). For the measurements Cu Kα1 radiation ($\lambda_{K\alpha 1} = 1.54056$ Å, $E_{K\alpha 1} = 8047.78$ eV, $U = 40$ kV, $I = 30$ mA) of an X-ray tube was used. The Ciclesonide powders were filled between mylar foil and adjusted in the path of rays for the transmission mode experiments.

The DSC scans of the investigated batches were carried out in a temperature range between 40 and 300°C on a dynamical differential scanning calorimeter of TA instruments (DSC Q1000) with dry nitrogen as purge gas (50 mL/min). A heating rate of 20 K/min were used for the determination of the calibration curves (amorphous content vs. recrystallization enthalpy), heating rate of 10, 20, 30, 50, and 100 K/min were used for the screening of the detection limit (1% amorphous content). Before performing the DSC sample scans, a T4P calibration (baseline, cell constant, onset slope, cp constant, indium melting point temperature calibration) was carried out for the heating rates 10, 20, and 100 K/min.

Thermogravimetric measurements were performed on a Hi-Res TGA 2950 thermogravimetric Analyzer from TA instruments. For each measurement about 5 mg of the substance were accurately weighed into a platinum TG pan. The weighed change of the sample was recorded in a

temperature range between 30 and 250°C applying a heating rate of 10 K/min. ^{1}H-NMR spectra of amorphous Ciclesonide were recorded in $CDCl_3$ on a Bruker 200 MHz-NMR spectrometer (DPX 200).

Dissolution Experiments

For each point in time (5, 10, 20, 35, 60, and 1440 min) of the dissolution experiment two samples were prepared by weighing about 15 mg of amorphous or crystalline Ciclesonide accurately into a conical Erlenmeyer flask and stirring (850 rpm) them at 37°C in 100 mL water (Millipore quality, ELIX 3, Gradient A 10). The moment of the addition of water was defined as t_0. The tempering of the samples was performed using an air bath. After the desired stirring time the complete samples were filtered over a 0.2 μm membrane filter (Schleicher & Schuell, Dassel, Germany, RC 0.2 μm Spartan 30/A) and concentrated on a Sep-Pak cartridge (Waters Sep-Pak cartridge C18, WAT051910). Afterwards the cartridge was eluted with ethanol (gradient grade, Merck, Darmstadt, Germany). The Ciclesonide in the ethanol solution was then quantified with HPLC (LaChrom®-HPLC System Series 7000, column: Zorbax SB phenyl, eluent: water/ethanol 38:62% (v/v) isocratic, column temperature: 60°C, injection volume: 50 μL, UV-detection at 243 nm) against an external standard.

Saturation Solubility Experiments

Amorphous or crystalline Ciclesonide (14–25 mg) were accurately weighed into a conical Erlenmeyer flask with rubber stopper ($n = 3$). Hundred milliliters of water (Millipore quality, ELIX 3, Gradient A 10) were added and 30 min ultrasonic treatment was applied to the samples (pH 5.9–6.0). Afterwards the samples were stirred in the dark for 24 h at 37°C in a water bath. After the desired stirring time each sample was completely filtered over a 0.2 μm membrane filter (Schleicher & Schuell, RC 0.2 μm Spartan 30/A) and concentrated on a Sep-Pak cartridge (Waters Sep-Pak cartridge C18, WAT051910). Then the cartridge was eluted with ethanol (gradient grade, Merck). The Ciclesonide in the ethanol solution was then quantified with HPLC (LaChrom®-HPLC System Series 7000, column: Zorbax SB phenyl, eluent: water/ethanol 38:62% (v/v) isocratic, column temperature: 60°C, injection volume: 50 μL, UV-detection at 243 nm) against an external standard.

Materials and Procedures

X-ray Amorphous Ciclesonide

For the preparation of amorphous Ciclesonide about 0.5 g crystalline Ciclesonide were dissolved in 70 mL 2-methyl-propan-2ol (tert-butanol), quench cooled in liquid nitrogen under stirring and lyophilized over 2 days, yielding the amorphous material. Amorphous Ciclesonide is a very light, voluminous powder. As tert-butanol was used as solvent for the lyophilization process it was of interest to quantify the amount of remaining tert-butanol in the lyophilized batches. Two quantification methods were established: (1) a thermogravimetrical method, which quantifies the tert-butanol content via a weight loss determination in the temperature range of 76–134°C and (2) a ^{1}H-NMR-spectrometrical method, which quantifies the tert-butanol content via the ratio of the integrals of the singulett proton signal of the three methyl-groups of tert-butanol (chemical shift: 1.27 ppm) and the signal of the olefinic H2 proton (chemical shift: 6.29 ppm) of Ciclesonide in the ^{1}H NMR-spectra. The results of both methods were in good agreement and showed that less than 0.6 w/w-% of tert-butanol was present in the samples used for the investigations.

Ciclesonide Samples with an Amorphous Content in the Range of 1–80 w/w-%

For the preparation of samples with a known amorphous content the appropriate amounts of crystalline and amorphous Ciclesoinde were accurately weighed and afterwards milled for 1 min at an amplitude of 30 with a Retsch Mixer mill MM 2000 (Retsch GmbH & Co. KG, Haan, Germany) using a 3 mL agate grinding jar equipped with an agate ball ($f = 0.70$ cm) and closed with a push-fit lid. The homogenized materials were stored in brown glass vessels in the dark at room temperature.

RESULTS AND DISCUSSION

Single-Crystal X-ray Diffraction, Dynamic Scanning Calorimetry (DSC), and FT-Raman Spectroscopy on Crystalline Ciclesonide

From polymorphism screening,[20] monitored by powder X-ray diffraction and FT-Raman spectroscopy, it is known that Ciclesonide exhibits only one polymorphic form. However, several solvates

(e.g., from tetrahydrofurane), so called pseudopolymorphic forms, are known.[20]

The colorless single crystals of Ciclesonide were obtained from a solution of Ciclesonide in a water–ethanol mixture (10 g Ciclesonide per 58 mL ethanol/water (1.7:1 v/v)). The crystal and molecular structure (Fig. 2) was assigned (Tab. 1). The orthorhombic needles belong to the space group $P2_12_12_1$ with lattice constants of $a = 6.638(1)$ Å, $b = 14.079(3)$ Å, $c = 32.870(7)$ Å, $\alpha = \beta = \gamma = 90^\circ$, and four independent molecules in the unit cell. The crystal structure obtained establishes the configuration of all chiral centers. As expected, the underlying steroid structure is approximately planar, with axial orientation of the substituents on C(10), C(11), and C(13). The side-chain on ring D is cis to the neighboring methyl group on C(13). Accordingly, the acetal moiety is trans to C(13). The cyclohexyl substituent on acetal carbon C(22) is cis (syn) to the steroid skeleton, giving the molecule a curved structure. Assuming that inversion of the configuration of all five carbon atoms of 16-α-hydroxyprednisolone, which is the starting material of the Ciclesonide synthesis, can be ruled out, the structure is that of 22R-Ciclesonide.

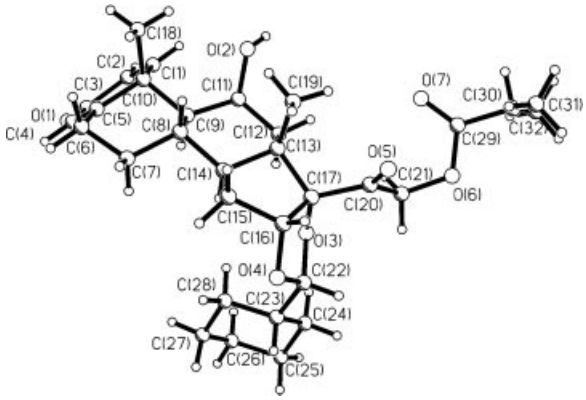

Figure 2. Molecular structure of Ciclesonide according single crystal X-ray diffraction.

Crystalline Ciclesonide exhibits a powder X-ray diffraction pattern with sharp Bragg reflexes up to an angular 2θ-range of 40° (in Fig. 3: data only depicted up to 30°). A simulated powder pattern of Ciclesonide according to the single crystal data,

Table 1. Crystal Data and Structure Refinement for Ciclesonide

Identification Code	Ciclesonide
Empirical formula	$C_{32}H_{44}O_7$
Formula weight	540.67
Temperature	293(2) K
Wavelength	0.71073 Å
Crystal system	Orthorhombic
Space group	P2(1)2(1)2(1)
Unit cell dimensions	$a = 6.6380(10)$ Å, $\alpha = 90^\circ$ $b = 14.079(3)$ Å, $\beta = 90^\circ$ $c = 32.870(7)$ Å, $\gamma = 90^\circ$
Volume	3071.9(10) Å^3
Z	4
Density (calculated)	1.169 g/cm^3
Absorption coefficient	0.081 mm^{-1}
$F(000)$	1168
Crystal size	$0.8 \times 0.015 \times 0.01$ mm^3
Theta range for data collection	1.90–24.39°
Index ranges	$-7 \le h \le 7$, $-16 \le k \le 16$, $-38 \le l \le 37$
Reflections collected	19500
Independent reflections	4730 [R(int) = 0.1350]
Completeness to theta = 24.39°	93.6%
Absorption correction	None
Refinement method	Full-matrix least-squares on F^2
Data/restraints/parameters	4730/0/353
Goodness-of-fit on F^2	0.764
Final R indices [$I > 2$sigma(I)]	R1 = 0.0494, wR2 = 0.0896
R indices (all data)	R1 = 0.1553, wR2 = 0.1187
Absolute structure parameter	−3(2)
Largest diff. peak and hole	0.149 and −0.114 e.Å^{-3}

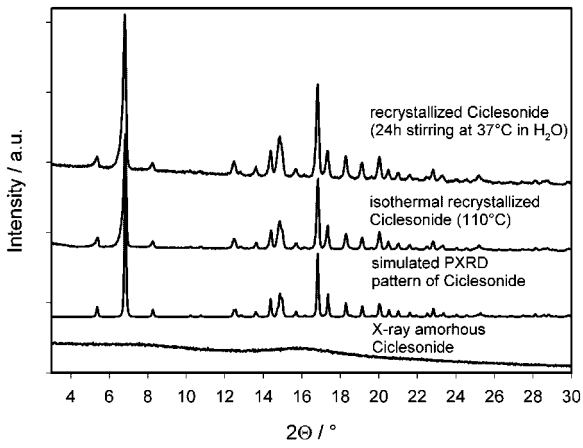

Figure 3. Powder X-ray diffraction patterns (transmission mode) of X-ray amorphous Ciclesonide, isothermally recrystallized (3.5 h at 110°C) Ciclesonide and solid residue from saturation solubility determination (24 h stirring in H_2O at 37°C) in comparison with the simulated powder diffraction pattern according single crystal data of Ciclesonide.

shown in Figure 3, is in excellent agreement with experimentally obtained patterns of crystalline Ciclesonide. DSC curves of crystalline Ciclesonide (heating rate: 10 K/min, refer to Fig. 4) show only one sharp endothermic signal caused by melting in a temperature range between 209 and 211°C ($\Delta H_f = 55 \pm 2$ J/g). The FT-Raman spectrum of crystalline Ciclesonide is shown in Figure 5 (spectrum on top). Possible assignments of some of the Raman signals to the vibrations are given in Table 2.

PXRD, DSC, and FT-Raman-Spectroscopy on X-ray Amorphous Ciclesonide

From a solution of Ciclesonide in 2-methyl-propan-2-ol (tert-butanol), which is quench cooled in liquid nitrogen under stirring and lyophilized over 2 days, amorphous Ciclesonide can be obtained. In contrast to the powder X-ray diffraction pattern of the crystalline Ciclesonide the lyophilized material shows only two broad maxima in its PXRD-patterns, while the sharp Bragg reflexes are completely missing (refer to Fig. 3). This observation indicates that the lyophilization process has produced a completely amorphous Ciclesonide. Due to particle size-dependent texture effects observed for crystalline Ciclesonide in reflection mode the PXRD experiments were performed in transmission mode. In the DSC curves of amorphous Ciclesonide two very strong signals can be detected: the exothermal recrystallization peak

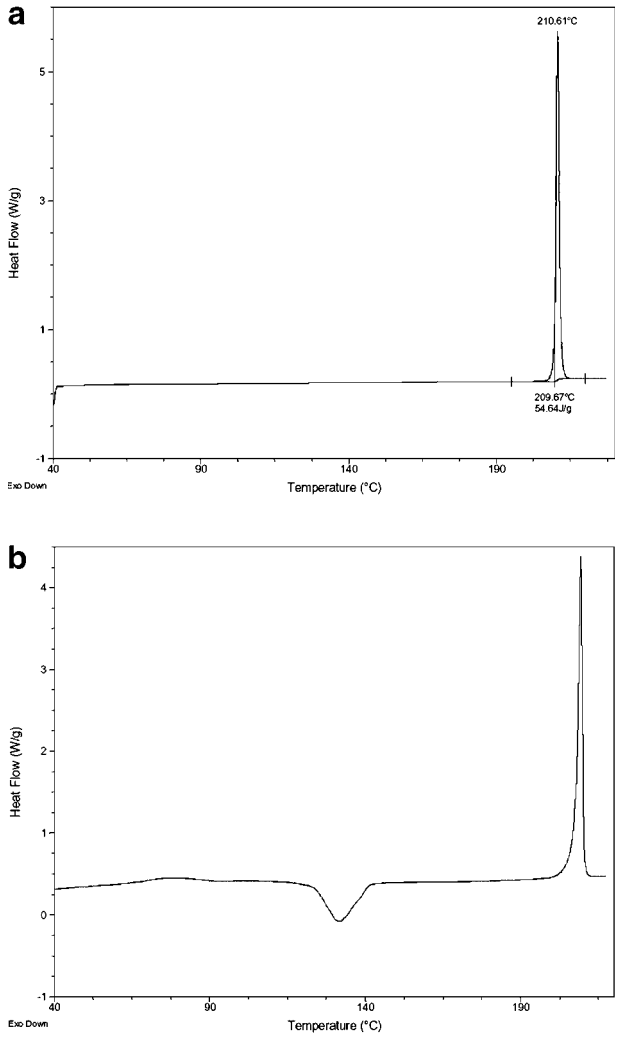

Figure 4. Differential scanning calorimetry (DSC) scan of (a) crystalline and (b) X-ray amorphous Ciclesoinde at a heating rate of 10 K/min.

and the endothermal melting signal (Fig. 4b). The broad exothermal signal in the temperature range between 60 and 100°C might be due to the liquid–gas phase transition process of the residual solvent tert-butanol. The determined heat of fusion of the amorphous material was found to be lower than the value for crystalline Ciclesonide. This finding corresponds with the observation, that the recrystallization enthalpy is also lower than the heat of fusion of pure crystalline material and might be explained by an incomplete recrystallization of amorphous Ciclesonide during the DSC experiments. The FT-Raman spectrum of amorphous Ciclesonide (Fig. 5) is significantly different from that of the crystalline material, as peak shifts, signal broadening, and changes in the intensity

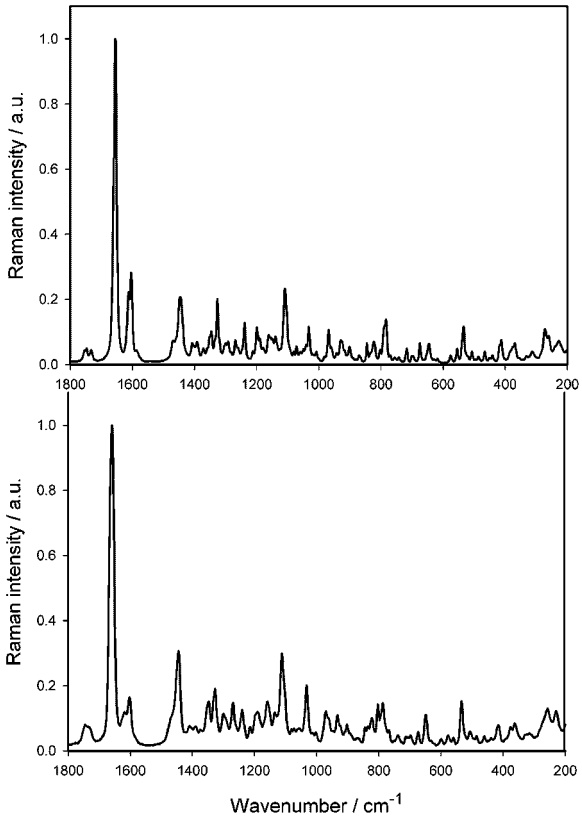

Figure 5. Comparison of the Fourier transformed (FT)-Raman spectra of crystalline (top) and amorphous (bottom) Ciclesonide, spectral resolution: 2 cm^{-1} (laser power: 100 mW, 512 scans), wavenumber range: 1800–120 cm^{-1}.

ratios were observed. Overall the yield of Raman-scattered photons at a certain laser power (100 mW) was found to be significantly lower in the amorphous Ciclesonide than in pure crystalline samples. The differences in the Raman spectra of both forms can be used for the detection and quantification of amorphous content in Ciclesonide batches. In Figure 6, comparison plots of the FT-Raman of Ciclesonide samples with amorphous contents between 0 and 100 w/w-% in different spectral regions are shown. These samples were prepared by spiking crystalline Ciclesonide with definite amounts of amorphous material. The homogenization of the samples was achieved by a ball-milling procedure. The milling conditions were kept as gentle as possible to avoid the formation of additional amorphous substance from crystalline material through the homogenization process. Two data analysis methods of the FT-Raman spectra were found to be suitable for quantification: (a) the plot amorphous content versus the intensity ratio $I(1604\ cm^{-1})/I(804\ cm^{-1})$ (method 1, Fig. 7a)) and (b) the plot amorphous content versus the shift of the Raman signal (refer to Fig. 6a) at half peak height (method 2, Fig. 7b). The calculation of the intensity ratio was performed from the "original" Raman spectra (without background correction). The data points of both plots can be fitted using a linear model ($Y = A + BX$). The rather big error bars of the data points in both plots can be explained by inhomogeneities within the samples. This is a general problem of quantification methods using calibration mixtures, which are obtained by mixing solid components with different morphological and physical characteristics. The investigation of such mixtures with spectroscopic method at high spatial resolution requires very high homogeneity. To obtain reliable results the repetition rate of the FT-Raman experiments was set to $n = 6$. The plot amorphous content versus the intensity ratio $I(1604\ cm^{-1})/I(804\ cm^{-1})$ showed a better linearity than the Raman signal shift plot. The limit of detection (LOD) and limit of quantitation (LOQ) for

Table 2. Assignments of the Signals in the Fourier Transformed (FT)-Raman Spectrum of Crystalline Ciclesonide

Wavenumber/cm^{-1}	Peak Type	Assignment
2968–2849	Strong, sharp	$-CH_2-$ and $-CH_3-$ asymmetric and symmetric stretching vibrations
1747, 1733	Weak, sharp	C=O stretching vibration of ketones and esters
1655	Strong, sharp	C=O stretching vibration of α, β-unsaturated carbonyl functions
1612, 1604	Medium, sharp	–C=C– stretching vibration of α, β-unsaturated carbonyl functions
1468–1346	Weak–medium, sharp	$-CH_2-$ and $-CH_3-$ asymmetric and symmetric deformation vibrations of methyl–, isopropyl, and cyclohexyl groups
1239	Weak, sharp	C–O stretching vibration in esters
1199–1032	Weak–medium, sharp	C–O stretching vibrations in secondary alcohols and asymmetric C–O–C–O–C stretching vibrations in acetals
823	Weak, sharp	C=C–C=O out of plane deformation vibration
784, 698	Weak, sharp	$-CH_2-$ rocking vibrations

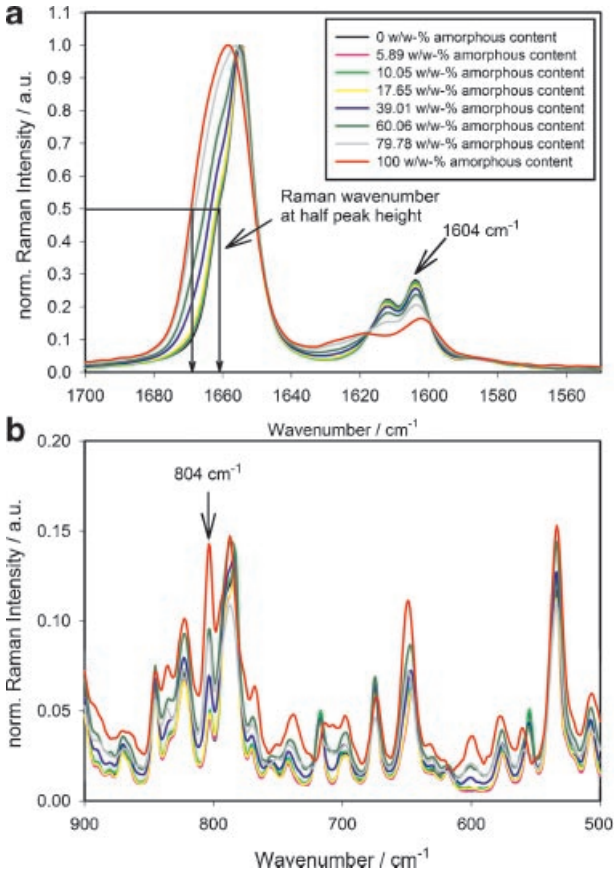

Figure 6. Comparison of the FT-Raman spectra of Ciclesonide batches with different amorphous content (crystalline Ciclesonide spiked with certain portions of X-ray amorphous material), spectral resolution: 2 cm^{-1} (laser power: 100 mW, 512 scans), wavenumber range: (a) 1700–1550 cm^{-1} and (b) 900–500 cm^{-1}.

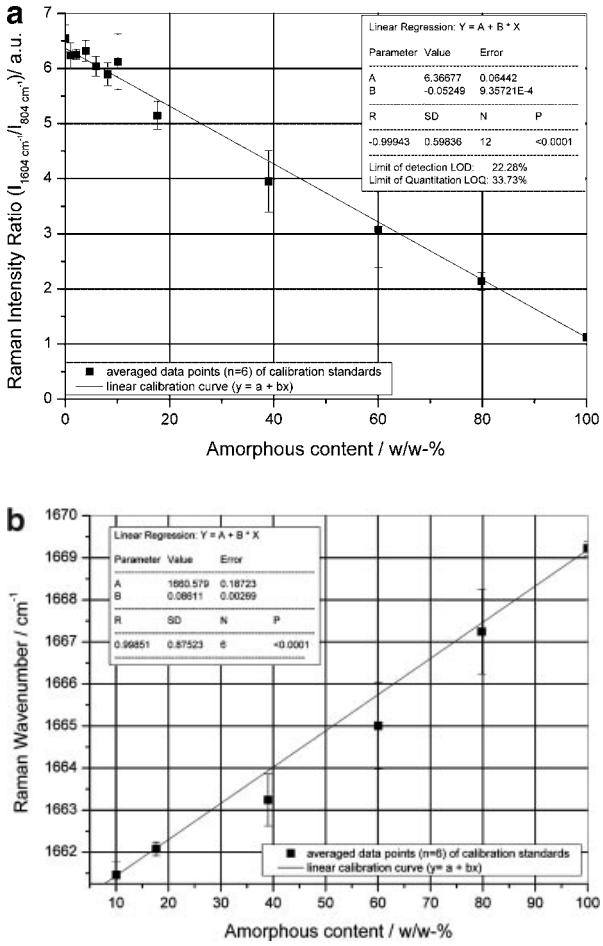

Figure 7. Calibration plots for spiked Ciclesonide samples: (a) FT-Raman intensity ratio $I_{1604\,cm^{-1}}/I_{804\,cm^{-1}}$ versus amorphous content and (b) FT-Raman wavenumber at half peak height versus amorphous content (refer to Fig. 6).

method 1 (quantification range: 0–100 w/w-%) is 22 and 33 w/w-%, respectively. Method 1 was applied for the calculation of relative crystallinities of amorphous Ciclesonide samples during hot-stage Raman experiments. A more accurate method to detect and quantify even small amounts of amorphous material was established by the use of DSC. In this case the calibration was performed with samples, which were produced by weighing the desired amounts of amorphous and crystalline Ciclesonide directly in an aluminum DSC pan without mixing them. These samples were measured using a heating rate of 20 K/min. The data in the plot of amorphous content (theoretical) versus recrystallization enthalpy $\Delta H_{\text{Recrystallization, corrected}}$ in the range between 0 and 10 w/w-% (18 data points) showed a very good linear behavior ($R^2 = 0.9948$, Fig. 8). Linear least squares fitting of the data resulted in an LOD of 0.7 w/w-% and an LOQ of 2.3 w/w-% amorphous content.

Comparison of the Thermodynamic Solubility and the Dissolution Behavior of Amorphous and Crystalline Ciclesonide

Ciclesonide is a highly lipophilic substance with a partition coefficient $\log P$ of 5.1 (=distribution coefficient at pH 7.4; $\log D$ (pH 7.4)) obtained by shake flask technique. Ciclesonide exhibits strong glass adsorption and a low solubility, thus special experimental care was taken, concerning recovery during the solubility and dissolution experiments. As Ciclesonide is neither protonated nor deprotonated (no pK_a values) within the physiologically and pharmaceutically relevant pH-range between

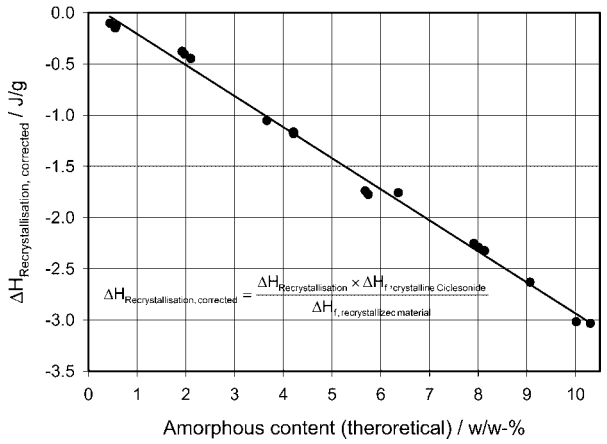

Figure 8. Calibration plot corrected recrystallization enthalpy measured by DSC (heating rate: 20 K/min, 18 data points between 0 and 11 w/w-% amorphous content) versus amorphous content (theoretical, according weighted sample).

1 and 12, the saturation solubility (thermodynamical solubility) of amorphous and crystalline Ciclesonide was determined in pure water (pH 5.9–6.0) after 30 min of ultrasonic treatment and additional 24 h of stirring at 37°C. The saturation concentration (c_s) of crystalline ($c_s = (1.67 \pm 0.05) \times 10^{-7}$ mol/L,) and amorphous ($c_s = 1.69 \pm 0.10) \times 10^{-7}$ mol/L) Ciclesonide are within the experimental error. For the reason of comparison the dissolution experiments were also carried out in pure water at 37°C under non-sink conditions (suspension; 15 mg substance in 100 mL water). The dissolution profiles of crystalline and amorphous Ciclesonide, monitored over 60 min with an additional data point at 24 h, are shown in Figure 9.

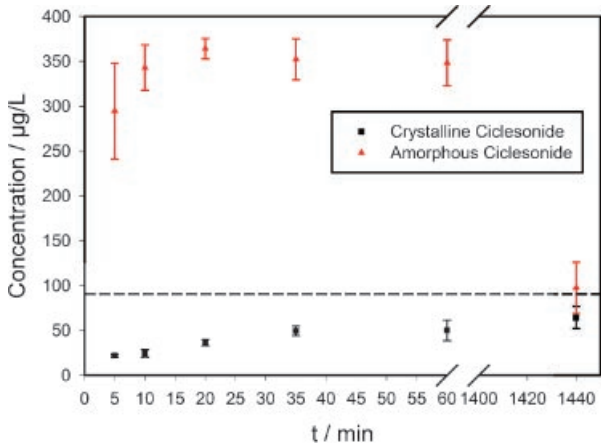

Figure 9. Dissolution behavior of crystalline (■) and amorphous (▲) Ciclesonide in water at 37°C monitored over 60 min and 24 h. The saturation solubilities of amorphous (91.6 ± 5.2 µg/L) and crystalline (90.1 ± 2.2 µg/L) Ciclesonide, measured in water at 37°C after 24 h of stirring, are marked as dashed line in the graph.

Within the first 60 min small amounts of crystalline Ciclesonide dissolve. The measured concentration after 60 min was 50 µg/L, significantly lower than the saturation solubility of crystalline Ciclesonide of (90.1 ± 2.2) µg/L. In the case of amorphous Ciclesonide a completely different situation was found. The concentration increased almost instantaneously to values, which were up to four times higher than the saturation solubility determined for amorphous Ciclesonide (91.6 ± 5.2 µg/L). After 24 h, however, the concentration in the dissolution experiments was found to be in agreement with the saturation concentration. Obviously amorphous Ciclesonide is, in comparison with the crystalline phase, able to form oversaturated solutions in water, which are stable for at least 60 min. The initial stability of the oversaturated solutions can be explained by the absence of inoculation crystals in the amorphous phase, which act as crystallization seeds in the slurry. This observation demonstrates that the dissolution rate of poorly soluble compounds can be increased by the preparation of an amorphous phase. In both dissolution experiments a white solid residue was obtained. The residue of the saturation solubility experiment of amorphous Ciclesonide in water was isolated by centrifugation. Dispersive Raman microscopy on the wet residue revealed that the spectrum of the material was in excellent agreement with crystalline and isothermally recrystallized Ciclesonide. The same finding was obtained applying powder X-ray diffractometry on this sample. The diffraction pattern of the residue from the solubility determination is shown in Figure 3 and is in perfect agreement with the simulated pattern, calculated from single crystal data. Thus it was demonstrated that amorphous Ciclesonide has precipitated in the known crystallographic form of Ciclesonide. This is the reason why crystalline and amorphous Ciclesonide exhibits the same saturation solubilities.

Kinetic Studies of the Recrystallization Process of Amorphous Ciclesonide Monitored by Dispersive Hot-Stage Raman Microscopy

The recrystallization of amorphous Ciclesonide can be either monitored by DSC experiments or through dispersive hot-stage Raman microscopy.

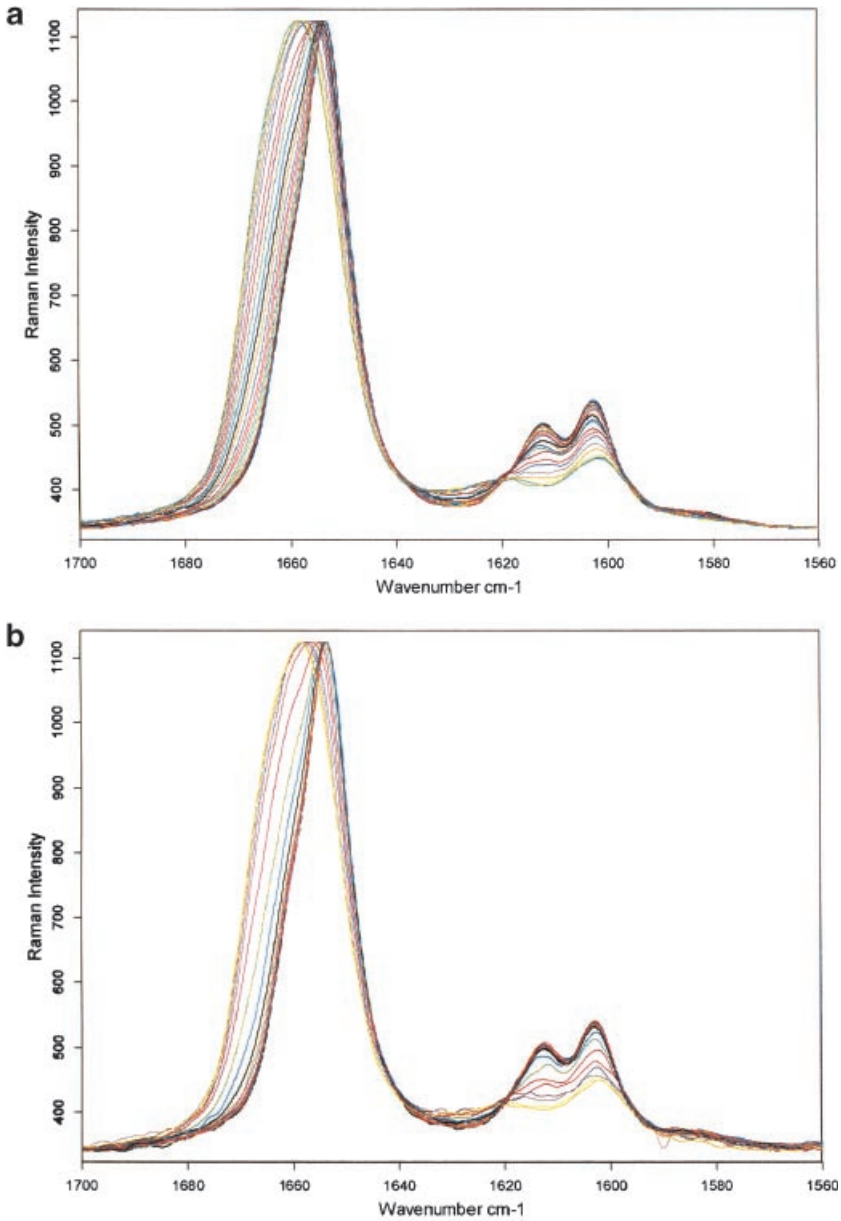

Figure 10. Recrystallization of amorphous Ciclesonide at constant temperatures of (a) 106°C (3. measurement) and (b) 110°C monitored over 146 min (time between the spectra: 5.4 min) by the normalized dispersive Raman spectra in the spectral region 1700–1560 cm^{-1}.

In Figure 10, the isothermal recrystallization of amorphous Ciclesonide at 106 and 110°C monitored by hot-stage Raman microscopy is shown. Again, like in the FT-Raman spectra in Figure 6, the typical shifts of the Raman signals as well as the changes in the intensity ratios can be observed in dependence of the crystallinity. The relative crystallinity X of the investigated sample at time t can be calculated from the Raman intensity ratio $I_{1604\,cm^{-1}}/I_{804\,cm^{-1}}$. This particular intensity ratio showed in the FT-Raman quantification of the amorphous content in spiked Ciclesonide samples a linear relationship with the crystallinity of the sample, thus it is possible to calculate the relative crystallinity by a careful determination of the intensity ratio for $X = 0$ and 100% and a linear interpolation between those points. In Figure 11, a comparison between a dynamical temperature scan monitored by dispersive hot-stage Raman microscopy

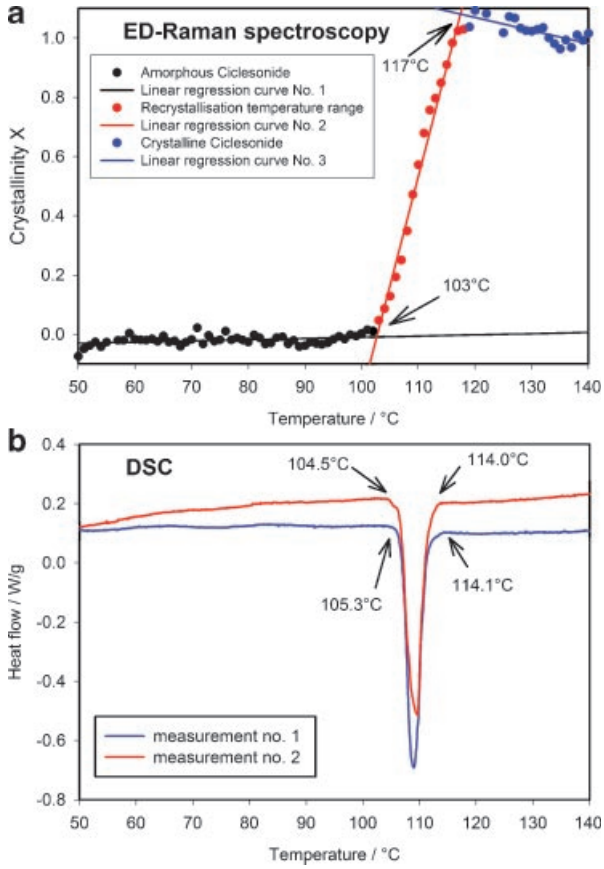

Figure 11. Recrystallization of X-ray amorphous Ciclesonide monitored by (a) a temperature versus relative crystallinity (X) plot obtained by an dispersive hot-stage Raman microscopic measurement (heating rate: 0.17 K/min; 5.4 min isothermal at each temperature) and (b) a temperature versus Heat flow plot obtained by DSC(heating rate: 2 K/min).

(heating rate: 0.17 K/min; 5.4 min isothermal at each temperature) and DSC (heating rate: 2 K/min) is shown. In the DSC curves the beginning of crystallization was found at a temperature of about 105°C, this is in agreement with the value obtained by dispersive Raman microscopy (103°C). Also the endpoints are in agreement in the order of magnitude.

A main characteristic of crystallization processes from a solid amorphous phase is the low mobility of the atoms or molecules. The system under investigation (amorphous Ciclesonide) already exhibits the chemical composition of the crystalline phase and is homogenous thus no long-range diffusion processes are necessary. Therefore, the crystallization process is determined by the formation of crystallization nuclei and interface controlled crystal growth. Several approaches and methods have been developed to analyze kinetic data from recrystallization processes, including fractal[21] and autocatalytic[22] models. Johnson, Mehl, and Avrami[23] developed model equations for phase transformations in which the metastable phase, in our case amorphous Ciclesonide, can coexist with a more stable phase (crystalline Ciclesonide) during the time of transformation.

The Avrami equation for isothermal crystallization is given by Eq. (1) or its double logarithmic form Eq. (2),[23b,c] where X_t is the relative crystallinity of the sample at the time t, n the so-called temperature-independent Avrami exponent and K a temperature-dependent parameter, comparable with a rate-constant. The Avrami exponent n varies for different nucleation and growth mechanisms[21,22,24] (refer to Tab. 3).

Deviations from the Avrami behavior might originate from the appearance of different growth mechanisms, impurities influencing the crystal growth, molecular mass distributions influencing the crystallization kinetics or the non-uniformity of the density of the growing phase.

$$X_t = 1 - e^{-Kt^n} \tag{1}$$

$$\ln\left(\ln\left(\frac{1}{1-X_t}\right)\right) = \ln(K) + n\,\ln(t) \tag{2}$$

Table 3. Avrami Exponents n for Different Nucleation (N) and Crystal Growth (CG) Mechanisms

$n_N + n_{CG} = n_{total}$	Description
1 + 0 = 1	Instantaneous nucleation + rodlike crystal growth
1 + 1 = 2	Random nucleation + rodlike crystal growth
2 + 0 = 2	Instantaneous nucleation + disclike crystal growth
2 + 1 = 3	Random nucleation + disclike crystal growth
3 + 0 = 3	Instantaneous nucleation + spheruliticlike crystal growth
3 + 1 = 4	Random nucleation + spheruliticlike crystal growth

In the case of amorphous Ciclesonide the isothermal recrystallization behavior at different temperatures can be followed by the changes in the Raman spectra (refer to Fig. 11) studied by energy dispersive hot-stage Raman microscopy. Isothermal recrystallization experiments were carried out at 65, 90, 100, 104, 106, 108, 110, 112, and 114°C. In Figure 11, it becomes evident that with increasing temperature the rate of recrystallization also increases. In the experiments which were carried out below 114°C a time lag between the beginning of the experiment and the first observation of recrystallization was found. The delay time was termed in this publication as t_{ind} (induction time). Such a time delay was described for several systems under investigation in the literature,[25–27] e.g., the recrystallization process of amorphous lactose at a relative humidity of 57.5% monitored by polarized light microscopy and gravimetry,[28] and associated with either the actual nucleation process and/or the slow growth of initial nuclei (germ nuclei). In Table 4, the experimentally obtained induction times of the different isothermal experiments along with their rather large standard deviations are given. In general the induction time increases with decreasing temperature. As the induction time shows strong temperature dependence an Arrhenius approach[26,28,29] can be made, which is expressed in Eq. (3) where A is a temperature-independent preexponential factor (min^{-1}), $\Delta E_{a,\ \text{induction time}}$ the activation energy (J/mol), R the gas constant (8.314 J mol^{-1} K^{-1}), and T the absolute temperature (K). Note that in this approach the reciprocal of the induction time is used for the Arrhenius plot.

$$\frac{1}{t_{ind}} = A \exp\left(-\frac{\Delta E_{a,\ \text{induction time}}}{RT}\right) \qquad (3)$$

Table 4. Observed Induction Time (t_{ind}) for Isothermal Recrystallization Experiments of X-Ray Amorphous Ciclesonide at 110, 90, 100, 104, 106, 108, 110, 112, and 114°C Monitored by Dispersive Hot-Stage Raman Microscopy

Temperature (°C)	t_{ind} (min)	$\ln(1/t_{ind})$
90	156.6 ($n = 1$)	−5.05
100	32.4 ± 7.6	−3.48
104	21.6 ± 5.4	−3.07
106	19.8 ± 2.0	−2.99
108	12.3 ± 3.4	−2.51
110	15.8 ± 5.0	−2.76
112	8.1 ($n = 1$)	−2.09
114	0	—

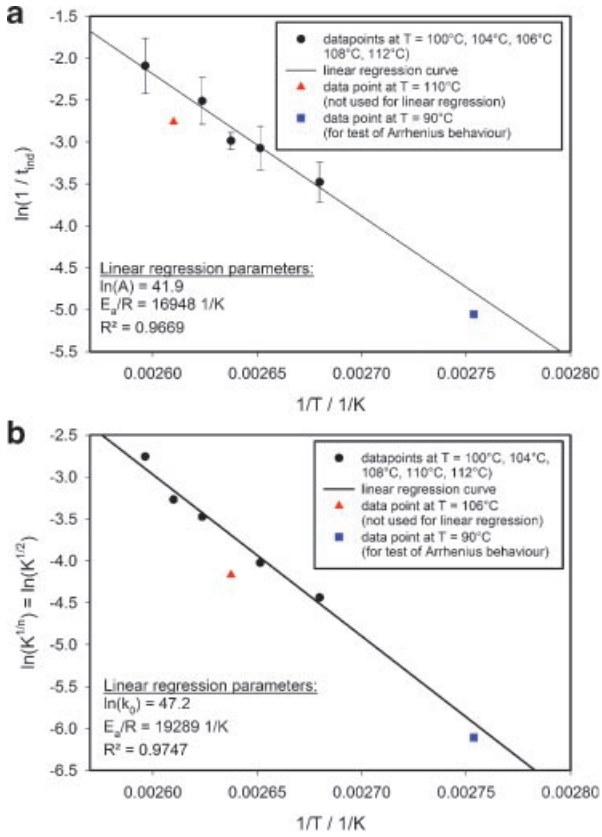

Figure 12. Arrhenius-type plots of (a) $\ln(1/t_{ind})$ versus $1/T$ using the $\ln(1/t_{ind})$-values of and (b) $\ln(K^{1/n})$ versus $1/T$ of the isothermal recrystallization of amorphous Ciclesonide using the K-values were the Avrami exponent was fixed at $n = 2$ (refer to Tab. 5). Linear regression of the data points in (a) marked as black circles gives an E_a/R-ratio of (16948 ± 1810) $1/K$ ($R^2 = 0.9669$), which leads to an activation energy $E_{a,\ \text{induction time}}$ of 140.9 ± 15.1 kJ/mol (33.7 ± 3.6 kcal/mol). Linear regression of the data points in (b) marked as black circles gives an E_a/R-ratio of 19289 $1/K$ ($R^2 = 0.9747$), which leads to an activation energy $E_{a,K}$ of (160.4 ± 14.9) kJ/mol ((38.4 ± 3.6) kcal/mol).

In Figure 12a, the Arrhenius plot of the experimental data, presented in Table 4, is given. The data points show a good linearity, therefore the line of best fit was calculated by least squares method in the temperature range between 100 and 112°C. From the obtained regression parameters the activation energy $\Delta E_{a,\ \text{induction time}}$ was calculated, giving a value of (140.9 ± 15.1) kJ/mol. The linear regression curve very well approximates the experimental data point (one measurement) at 90°C, thus the assumed Arrhenius behavior is very likely.

Coming back to the actual recrystallization process (crystal growth), which can be followed by

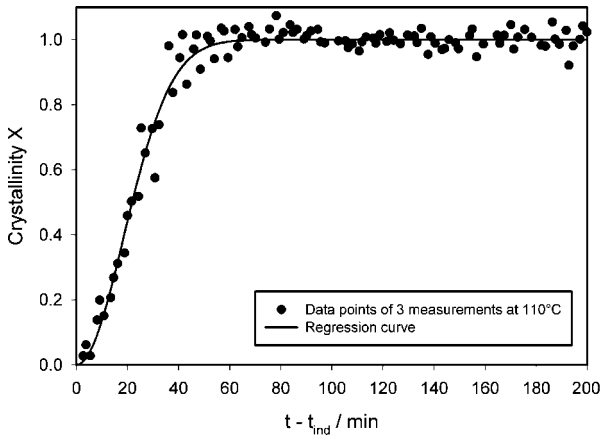

Figure 13. Avrami plot of three independent experiments at 110°C. For the fitting procedure the Avrami exponent was fixed to $n = 2$, in order to reduce the number of free parameters.

the spectral changes in the Raman spectra. Figure 13 shows the changes in crystallinity of amorphous Ciclesonide at 110°C in dependence of the time corrected by the induction time (t–t_{ind}). The data points of three independent isothermal measurements (110°C) are shown. The solid line in this figure represents the fitted Avrami curve (according Eq. (1); $n = 2$). This process can be done for all isothermal experiments. The calculated Avrami parameters for the different temperatures are listed in Table 5. In general an Avrami exponent of about two was observed, indicating either a random nucleation with a followed rodlike crystal growth or an instantaneous nucleation with a followed disclike crystal growth. The obtained K values, however, did not show the expected steady rise with increasing temperature. Therefore and in order to reduce the number of free parameters a second fitting procedure was performed by fixing the Avrami exponent to a value of 2. The results are also given in Table 5. By fixing the n-value to two, the expected K behavior in dependence of temperature was gained. A graphical overview over the fitted Avrami curves with fixed Avrami exponent ($n = 2$) at different temperatures is shown in Figure 14. It becomes evident that with increasing temperatures the recrystallization process becomes faster.

As mentioned, the rate constant K is a temperature-dependent parameter. Therefore, this parameter can be used, likewise already demonstrated with the induction time, to determine activation energies of crystallization. The temperature dependence of K can be described by an Arrhenius function,[30–32] given by Eq. (4), where k_0 is a temperature-independent preexponential factor (min^{-1}), $\Delta E_{\mathrm{a},K}$ the activation energy (J/mol), R the gas constant (8.314 J mol^{-1} K^{-1}), T the absolute temperature (K), and n the Avrami exponent (in our case $n = 2$).

$$K^{1/n} = k_0 \exp\left(-\frac{\Delta E_{\mathrm{a},K}}{RT}\right) \tag{4}$$

The Arrhenius plot $\ln(K)$ versus $1/T$ (for data refer to Tab. 5) is shown in Figure 12b). A good linearity of the data points can be observed. The line of best fit was calculated by least squares method in the temperature range between 100 and 112°C. The determined activation energy $\Delta E_{\mathrm{a},K}$ is (160.4 ± 14.9) kJ/mol, a value rather similar to that calculated from the temperature dependence of the induction time. The experimental data point at 90°C (Fig. 12b) is very well predicted by the regression curve, thus giving evidence for the Arrhenius behavior.

CONCLUSION

In this work the single crystal structure of Ciclesonide was solved. The orthorhombic needles of Ciclesonide crystallize in $P2_12_12_1$ space group with four independent molecules in the unit cell. A lyophilization process for the preparation of X-ray amorphous Ciclesonide was established, in order to obtain a drug material, which differs in its physicochemical properties from the crystalline form.

FT-Raman spectroscopic and DSC methods were developed in order to determine low amorphous content in crystalline samples. Both methods can be used for the determination of amorphous content in crystalline drug products. Nevertheless, the DSC method (LOD: 0.7 w/w-%; LOQ: 2.3 w/w-%) was found to be much more sensitive and accurate than the determination via FT-Raman spectroscopy. This is mainly due to the problem of the preparation of homogenous mixtures of crystalline material spiked with increasing portions of amorphous substance, necessary for the FT-Raman spectroscopic method. Therefore, within these two methods DSC might be seen as the method of choice for the accurate quantification of low amounts of amorphous material.

From dissolution experiments, carried out in water at 37°C on crystalline and amorphous Ciclesonide, it became evident that

Table 5. Determination of Avrami Exponents (n) from Non-Linear Regression of the Avrami Plots $X(t) = 1 - \exp(-K \cdot t^n)$ of the Isothermal Recrystallization of X-Ray Amorphous Ciclesonide at 90, 100, 104, 106, 108, 110, 112, and 114°C Monitored by Dispersive Hot-Stage Raman Microscopy

Measurement No./t_{ind}	n	K (min^{-n})	R^2
$T = 90$°C (heating rate: 10°C/min to 90°C)			
1/156.6 min	1.96	0.0000064	0.9957
All data points fit (n fixed)	2	0.0000050	0.9958
$T = 100$°C (heating rate: 10°C/min to 100°C)			
1/37.8 min	1.26	0.0038	0.9921
2/27.0 min	1.94	0.0002	0.9948
Average ± standard deviation	1.6 ± 0.5	0.0020 ± 0.0025	
All data points fit	1.6	0.00100	0.9867
All data points fit (n fixed)	2	0.00014	0.9785
$T = 104$°C (heating rate: 10°C/min to 104°C)			
1/21.6 min	2.00	0.0002	0.9975
2/16.2 min	1.64	0.0018	0.9928
3/27.0 min	1.50	0.0025	0.9969
Average ± standard deviation	1.7 ± 0.3	0.0015 ± 0.0012	
All data points fit	1.7	0.00120	0.9759
All data points fit (n fixed)	2	0.00032	0.9714
$T = 106$°C (heating rate: 10°C/min to 106°C)			
1/22.1 min	1.50	0.0011	0.9911
2/18.7 min	1.81	0.0008	0.9952
3/18.7 min	1.61	0.0011	0.9957
Average ± standard deviation	1.6 ± 0.2	0.0010 ± 0.0002	
All data points fit	1.6	0.00110	0.9453
All data points fit (n fixed)	2	0.00024	0.9387
$T = 108$°C (heating rate: 10°C/min to 108°C)			
1/16.2 min	2.34	0.0004	0.9807
2/10.8 min	2.61	0.0001	0.9961
3/10.0 min	2.60	0.0001	0.9791
Average ± standard deviation	2.5 ± 0.2	0.0002 ± 0.0002	
All data points fit	2.5	0.00020	0.9795
All data points fit (n fixed)	2	0.00096	0.9760
$T = 110$°C (heating rate: 10°C/min to 110°C)			
1/13.5 min	2.26	0.0006	0.9432
2/12.4 min	1.99	0.0017	0.9581
3/21.6 min	1.78	0.0030	0.9876
Average ± standard deviation	2.0 ± 0.2	0.0018 ± 0.0012	
All data points fit	2.0	0.0015	0.9795
All data points fit (n fixed)	2	0.0015	0.9795
$T = 112$°C (heating rate: 10°C/min to 112°C)			
1/8.1 min	1.39	0.0211	0.9935
All data points fit (n fixed)	2	0.0040	0.9742
$T = 114$°C (heating rate: 10°C/min to 114°C)			
1/0 min	—[a]	—[a]	—[a]

R^2, squared multiple correlation coefficient of linear regression; t, time in s.
[a] After third datapoint crystallinity was found to be 100% (no Avrami evaluation possible).

amorphous Ciclesonide tends to form oversaturated solutions and exhibits initially faster dissolution behavior than the crystalline form, even if the saturation concentrations in water (after 24 h of stirring) of both forms ($c_{s,\ \text{crystalline Ciclesonide}} = 1.67 \times 10^{-7}$ mol/L) were found to be the same. The oversaturation effect of amorphous Ciclesonide might be used to achieve a a higher bioavailability of the drug.

It was demonstrated that the recrystallization process of amorphous Ciclesonide can be detected and quantified by either DSC or hot-stage Raman microscopy. Dispersive hot-stage Raman microscopy was successfully applied to study the

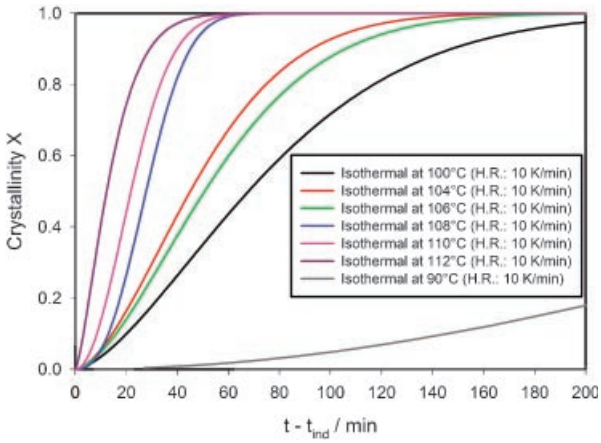

Figure 14. Comparison plot crystallinity of the fitted Avrami functions of the isothermal recrystallization of amorphous Ciclesonide at 90, 100, 104, 106, 108, 110, and 112°C versus time.

recrystallization kinetics of amorphous Ciclesonide. Thus hot-stage Raman microscopy can be seen as a new and good alternative to the well-established PXRD and DSC methods for the quantitative analysis of phase transition processes. We have also successfully applied hot-stage Raman microscopy on the crystalline hydrate form of another drug substance, to get an inside on the kinetics of the "drying" process (solid–solid form transition) to the crystalline anhydrate form.

The recrystallization of amorphous Ciclesonide was found to be a two-step process, most likely a nucleation process, detected by the presence of an induction time, followed by the actual crystal growth process, which was monitored by the spectral changes in the Raman spectra. The data of isothermal Raman experiments carried out at various temperatures were fitted to an Avrami model. The observed Avrami exponent of two can be interpreted in two different ways, either as a random nucleation with rodlike crystal growth or as an instantaneous nucleation with disclike crystal growth (2-dimensional process). The detection of an induction time as well as the crystal shape of crystalline Ciclesonide (needles) might be hints for the first of the two possible interpretations. As the induction times as well as the rate constants K followed an Arrhenius behavior both processes must be assumed to be thermally activated. From the Arrhenius plots it was possible to determine activation energies for both processes. The activation energies $E_{\mathrm{a,\ induction\ time}} = 140.9$ kJ/mol and $E_{\mathrm{a},K} = 160.4$ kJ/mol, respectively, lie in a rather similar energy range and are comparable with activation energies found for other organic systems, e.g., recrystallization of amorphous lactose ($E_{\mathrm{a},K} = 186.5$ kJ/mol, $E_{\mathrm{a,\ nucleation}} = 317$ kJ/mol), in the literature.[28] From the data obtained from the Arrhenius plots it becomes evident that below 60°C the recrystallization process of amorphous Ciclesonide is so slow ($\ln(K^{1/2}) < -10$) that the amorphous form can be considered as stable. This result is important to know for the manufacturing process (possible drying temperature range) as well as for considerations of the optimal storage temperature of the amorphous drug substance.

Overall it can be concluded that hot-stage Raman microscopy is a powerful tool for the identification and quantification of phase transition processes of solid drug substances.

ACKNOWLEDGMENTS

The authors would like to thank their laboratory staff, namely Sonja Prall, Brigitte Bössenecker, Collin Hoffmann, Ulrike Richter, Thomas Trebing, and Nina Keitel, for experimental support. Martin P. Feth is grateful to Dr. Rotraut Merkle, Max Planck Institute for Solid State Research, Stuttgart, for fruitful discussion. Furthermore, we wish to thank Prof. Dr. U. Kazmaier and Dr. V. Huch, Universität des Saarlandes, for the single-crystal X-ray diffraction experiments and Dr. M. Ermrich for the powder X-ray diffraction measurements and pattern simulations.

REFERENCES

1. Mullins JD, Mack TJ. 1960. Some pharmaceutical properties of novobiocin. J Am Pharm Assoc 49:245–248.
2. Shefter E, Higuchi T. 1963. Dissolution behaviour of crystalline solvated and nonsolvated forms of some pharmaceuticals. J Pharm Sci 52:781–791.
3. Fukuoka E, Makita M, Yamamura S. 1986. Some physicochemical properties of glassy indomethacin. Chem Pharm Bull 34:4314–4321.
4. Fukuoka E, Makita M, Yamamura S. 1987. Glassy state of pharmaceuticals. II. Bioinequivalence of glassy and crystalline indomethacin. Chem Pharm Bull 35:2943–2948.
5. Hancock BC, Parks M. 2000. What is the true solubility advantage for amorphous pharmaceuticals? Pharm Res 17:397–404.
6. Hancock BC, Zografi G. 1997. Characteristics and significance of the amorphous state in pharmaceutical systems. J Pharm Sci 86:1–12.

7. Craig DQM, Royall PG, Kett VL, Hopton ML. 1999. The relevance of the amorphous state to pharmaceutical dosage forms: Glassy drugs and freeze dried systems. Int J Pharm 179:179–207.
8. Zhou D, Zhang GGZ, Law D, Grant DJW, Schmitt EA. 2002. Physical stability of amorphous pharmaceuticals: Importance of configurational thermodynamic quantities and molecular mobility. J Pharm Sci 91:1863–1872.
9. Taylor LS, Zografi G. 1998. The quantitative analysis of crystallinity using FT-Raman spectroscopy. Pharm Res 15:755–761.
10. Palmer KJ, Dye WB, Black D. 1956. Sugar crystallization, X-ray diffractometer and microscopic investigation of crystallization of amorphous sucrose. J Agric Food Chem 4:77–81.
11. Hogan SE, Buckton G. 2001. The application of near infrared spectroscopy and dynamic vapor sorption to quantify low amorphous contents of crystalline lactose. Pharm Res 18:112–116.
12. Darcy P, Buckton G. 1998. Quantitative assessments of powder crystallinity: Estimates of heat and mass transfer to interpret isothermal microcalorimetry data. Thermochim Acta 316:29–36.
13. Briggner L-E, Buckton G, Bystorm K, Darcy P. 1994. The use of isothermal microcalorimetry in the study of changes in crystallinity induced during the processing of powders. Int J Pharm 105:125–135.
14. Hogan SE, Buckton G. 2000. The quantification of small degrees of disorder in lactose using solution calorimetry. Int J Pharm 207:57–64.
15. Saunders M, Podluii K, Shergill S, Buckton G, Royall P. 2004. The potential of high speed DSC (Hyper-DSC) for the detection and quantification of small amounts of amorphous content in predominantly crystalline samples. Int J Pharm 274: 35–40.
16. Saklatvala R, Royal PG, Craig DQM. 1999. The detection of amorphous material in a nominally crystalline drug using modulated temperature DSC—A case study. Int J Pharm 192:55–62.
17. Guinot S, Leveiller F. 1999. The use of MTDSC to assess the amorphous phase content of a micronised drug substance. Int J Pharm 192:63–75.
18. Stubberud L, Forbes RT. 1998. The use of gravimetry for the study of the effect of additives on the moisture-induced recrystallisation of amorphous lactose. Int J Pharm 163:145–156.
19. Sheldrick GM. 1997. SHELXK-97: A program for crystal structure determination. Göttingen, Germany: Universität Göttingen.
20. SSCI Inc., West Lafayette, IN, USA, 2005. Standard Polymorph Screen of Cilcesonide on behalf of ALTANA Pharma AG, Constance. Unpublished data.
21. (a) Liu XY, Sawant PD. 2002. Mechanism of the formation of self-organized microstructures in soft functional materials. Adv Mater 14:421–426.
(b) Liu XY, Sawant PD. 2001. Formation kinetics of fractal nanofiber networks in organogels. Appl Phys Lett 79:3518–3520.
22. Terech P. 1985. Kinetics of aggregation in a steroid derivative/cyclohexane gelifying system. J Colloid Interface Sci 107:244–255;
23. (a) Johnson WA, Mehl RF. 1939. Reaction kinetics in processes of nucleation and growth. Trans Am Inst Min Eng 135:416–441.
(b) Avrami M. 1939. Kinetics of phase change I. J Chem Phys 7:1103–1112.
(c) Avrami M. 1940. Kinetics of phase change. II: Transformation-time relations for random distribution of nuclei. J Chem Phys 8:212–224.
(d) Avrami M. 1941. Granulation, phase change, and microstructure kinetics of phase change III. J Chem Phys 9:177–184.
(e) de Bruijn TJW, Jong WA, van den Berg PJ. 1981. Kinetic parameters in Avrami—Erofeev type reactions from isothermal and non-isothermal experiments. Thermochim. Acta 45:315–325.
24. (a) Schultz JM. 1974. In Polymer Material Science;. Englewood Cliffs, New Jersey: Prentice Hall, p. 385.
(b) Wunderlich B. 1976. Crystal nucleation, growth, annealing. In: Macromolecular Physics. Vol. 2, New York: Academic Press. pp. 16–52, 147.
(c) Sharples A. 1966. Overall kinetics of crystallization. In: Introduction to Polymer Crystallization. London: Edward Arnold Ltd., pp. 44–59.
25. van Scoik KG, Carstensen JT. 1990. Nucleation phenomena in amorphous sucrose systems. Int J Pharm 58:185–196.
26. Bishop DW, Thomas PS, Ray AS, Šimon P. 2001. Two-stage kinetic model for the α–β phase recrystallisation in nickel sulphide. J Therm Anal Calorim 64:201–210.
27. Jacobs PWM. 1997. Formation and growth of nuclei and the growth of interfaces in the chemical decomposition of solids: New insights. J Phys Chem B 101:10086–10093.
28. Schmitt EA, Law D, Zhang GGZ. 1999. Nucleation and crystallization kinetics of hydrated amorphous lactose above the glass transition temperature. J Pharm Sci 88:291–296.
29. Isaev AI, Deng JS. 1988. Nonisothermal vulcanization of rubber compounds. Rubber Chem Technol 61:340–361.
30. Cebe P, Hong SD. 1986. Crystallization behaviour of poly(ether-ether-ketone). Polymer 27:1183–1192.
31. Zhu X, Li Y, Yan D, Fang Y. 2001. Crystallization behavior of partially melting isotactic polypropylene. Polymer 42:9217–9222.
32. Li Y, Zhang G, Zhu X, Yan D. 2003. Isothermal and nonisothermal crystallization kinetics of partially melting nylon 10 12. J Appl Polym Sci 88:1311–1319.